Orientation and Crystallinity in Film Casting of Polypropylene

GAETANO LAMBERTI, VALERIO BRUCATO, GIUSEPPE TITOMANLIO

Department of Chemical and Food Engineering, University of Salerno, Via Ponte don Melillo, 84084 Fisciano (SA), Italy

Received 23 January 2001; accepted 24 August 2001

ABSTRACT: In the cast film process a polymer melt is extruded through a slit die, stretched in air, and cooled on a chill roll. During the path in air the melt cools while being stretched. Film casting experiments were carried out with an isotactic polypropylene resin. The temperature and width distributions were measured along the draw direction. Further, the crystallinity and Hermans orientation factor were measured on the final film. The process was described by a simple thermomechanical model derived elsewhere. The evolution of the molecular orientation parameters was calculated on the basis of a dumbbell model coupled with velocity and temperature distributions provided by the thermomechanical model. The experimental crystalline orientations of the final films collapsed into a single step-shaped curve (from low to high orientation) if plotted versus the stress calculated by the model at the frozen line. The experimental values of the crystallinity and Hermans orientation factors are discussed on the basis of predictions of the dumbbell model for melt orientation at the frozen line and the crystallinity data obtained in quiescent conditions under the same cooling rate. © 2002 Wiley Periodicals, Inc. J Appl Polym Sci 84: 1981–1992, 2002; DOI 10.1002/app.10422

Key words: orientation; crystallinity; polypropylene; molecular modeling; film casting

INTRODUCTION

Thin plastic film production is a transformation process of great importance in polymer manufacturing. The first attempts to model the film casting of a viscous material in isothermal conditions were made by Pearson,[1] Narayanaswamy,[2] and Agassant et al.[3] Nonisothermal effects were accounted for in more recent articles by Duffo et al.,[4] Barq et al.,[5] and Acierno et al.[6] Their models were again based on viscous rheological constitutive equations. Lamberti et al.[7,8] also described the film casting process of a viscous semicrystalline polymer by a simple model, which was based on mass, momentum, and energy balance for a viscous fluid, accounting for crystallization kinetics and the effect of crystallinity on the viscosity.

It is known that the orientation of macromolecules due to flow leads to an increase of the crystallization kinetics.[9,10] However, despite the large amount of experimental works investigating the flow induced crystallization (FIC) phenomena, an effective modeling of the FIC kinetics was not achieved. Starting from early work by McHugh[10] and until more recent results, the proposed models are generally difficult to apply to practical cases[11] or require a large number of adjustable parameters.[12–14]

The study of orientation evolution by the effect of the flow during a process is thus still an up to

Correspondence to: G. Lamberti (glamberti@unisa.it).

Journal of Applied Polymer Science, Vol. 84, 1981–1992 (2002)

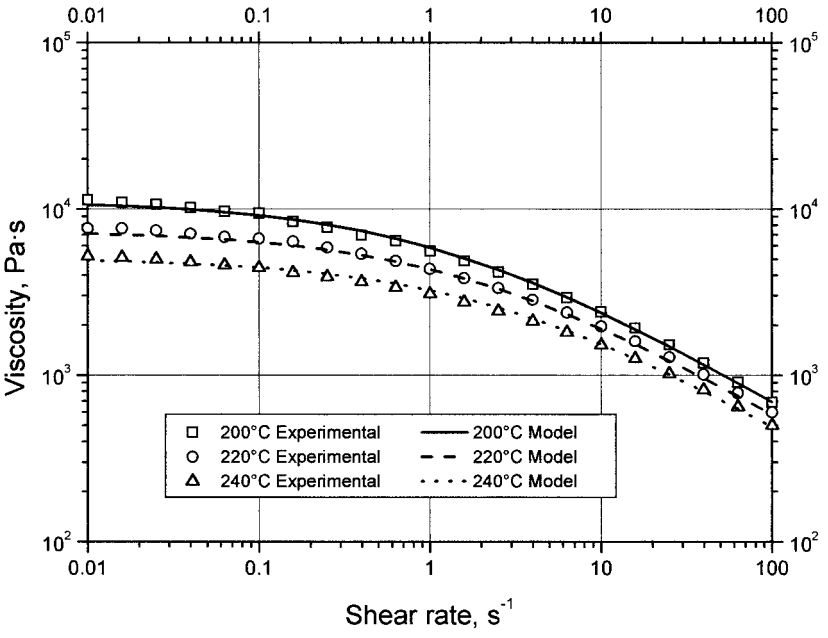

Figure 1 The experimental viscosity of iPP T30G at different temperatures. The curves are a prediction of the Cross model for the values of the parameters given in Table I.

date topic that is of relevant interest for the description of the effect of flow on crystallization kinetics during polymer processing.

The aim of this work is the identification of flow effects that takes place during the cast film process on the crystallinity and orientation of final films. The evolution of molecular orientation is also obtained on the basis of a dumbbell model and discussed in relation to the final film orientation.

EXPERIMENTAL

Materials

The resin adopted for experimental work is a commercial isotactic polypropylene (iPP) supplied by Montell (T30G, M_w = 483,000, M_n = 75,500).

Rheological characterization was carried out by shear rotational viscosimeters operated in oscillatory mode.[15] The Cox and Merz rule was applied to the oscillatory results. The viscosity of the material was described by the Cross equation:

$$\mu(T, \dot{\gamma}, X_c) = \frac{\mu_0(T)}{1 + [\mu_0(T)C\dot{\gamma}]^{1-nC}}\, \mu_{X_c}(X_c) \quad (1)$$

The temperature dependence is described by an activation energy (E_a):

$$\mu_0(T) = \mu_{0,r}\exp\left(\frac{E_a}{RT}\right) \quad (2)$$

Fitting of eq. (1) to experimental data is shown in Figure 1 for three different temperatures.

The factor $\mu_{X_c}(X_c)$ accounts for the effect of crystallinity on the viscosity; the expression suggested by Titomanlio et al.[16] was adopted for it:

$$\mu_{X_c}(X_c) = \left[1 + f\exp\left(-\frac{h}{X_c^m}\right)\right] \quad (3)$$

Equation (3) is such that $\mu_{X_c}(X_c)$ remains close to unity while X_c reaches a critical crystallinity value and then grows very fast; parameters were chosen so as to have a sharp increase of viscosity at X_c = 0.05, which assumes the meaning of a crystallinity solidification index (CSI). The values adopted for the parameters are given in Table I.

The crystallization kinetic data, which were obtained by cooling samples of the resin in a wide range of cooling rates by means of both a DSC apparatus and a home-made quenching device; were described[17] by the nonisothermal formulation of the Avrami equation attributable to Nakamura et al.[18]

More quenching and DSC experiments were added in this work. The crystallinity of the final

Table I Rheological Parameters for Use in Eq. (1)

$\mu_{0,r}$ (Pas)	E_a/R (K)	C (Pa^{-1})	nC	f	m	h	CSI
0.4196	4822.0	7.65×10^{-5}	0.389	2000	1.2	0.2	5%

samples determined by the FTIR method, which were calibrated in the new experiments, are in good agreement with previous crystallinity values obtained from density measurements reported by Piccarolo et al.[17]

Methods

Cast film extrusion was performed with a laboratory-scale extruder equipped with a take-up unit. An extrusion temperature of 473 K and two different rectangular dies with the same width (L_0 = 0.20 m) and different thicknesses (S_0 = 0.0005, and 0.0002 m) were adopted for all tests. Tests were performed adopting several values of extrusion screw rpms, take-up velocity, and distance X (X = 0.3 and 0.4 m) between the extrusion head and take-up rolls. All runs and relative relevant measured parameters are reported in Table II.

The mass flow rate ($\dot{m}$) was measured by extrudate weighting. The extrusion velocity [v_x (x = 0)] was calculated from the mass flow rate and melt density evaluated at the die temperature. The take-up velocity [v_x ($x = X$)] was simply evaluated from the collected film length.

Width and temperature profiles along the draw direction were measured for all tests. The width distribution along the draw direction was obtained by photographic acquisition and subsequent image analysis. In order to avoid any contact with the flowing melt, online temperature measurements were performed by IR pyrometry.

The crystallinity and Herman orientation factor were determined on final film samples by analysis of the FTIR absorption and IR dichroism. The crystallinity index was determined by the analysis of the absorbance of selected peaks[19] of the FTIR spectra on the basis of Lambert and Beer's law:

$$X_c = \frac{A(\nu_c)}{A(\nu_c) + \dfrac{a(\nu_c)}{a(\nu_{am})} A(\nu_{am})} \tag{4}$$

where ν_c and ν_{am} denote the wavenumbers of the absorbance peaks due to crystalline (ν_c = 841 cm^{-1}) and amorphous (ν_{am} = 973 cm^{-1}) fractions, respectively; $a(\nu_c)$, $a(\nu_{am})$, $A(\nu_c)$, and $A(\nu_{am})$ denote the absorptivity coefficients and measured absorbances at different wavenumbers, respectively.

The ratio $a(\nu_c)/a(\nu_{am})$ was estimated by calibration by means of density determinations on sam-

Table II Experimental Runs, Operative Conditions, and Relevant Measured Parameters

No.	Ω (rpm)	$\dot{m}$ (10^{-4} kg s^{-1})	v_{x0} (10^{-3} m s^{-1})	v_{xX} (10^{-3} m s^{-1})	X (m)	T_0 (°C)	S_0 (μm)	DR	f_c	$f_{a\nu}$	X_c
G1	60	4.00	13.28	95.3	0.30	200	200	7.2	0.019	0.001	0.518
G2	50	3.61	11.98	81.0	0.30	200	200	6.8	0.013	0.010	0.442
G3	40	2.83	9.40	79.7	0.30	200	200	8.5	0.020	0.017	0.439
G4	30	2.16	7.18	79.3	0.30	200	200	11.0	0.058	0.048	0.472
G5	20	1.47	4.87	77.3	0.30	200	200	15.9	1.000	0.638	0.621
G6	10	0.75	2.49	75.8	0.30	200	200	30.5	1.000	0.579	0.622
H6	40	2.89	3.83	80.2	0.40	200	500	20.9	0.038	0.040	0.541
H1	30	2.22	2.94	76.0	0.40	200	500	25.8	0.707	0.547	0.601
H5	25	1.80	2.39	75.0	0.40	200	500	31.3	0.805	0.552	0.612
H2	20	1.48	1.97	82.8	0.40	200	500	42.1	0.836	0.606	0.632
H4	15	1.13	1.50	82.3	0.40	200	500	54.7	0.868	0.658	0.622
H3	10	0.88	1.16	93.3	0.40	200	500	80.4	0.985	0.724	0.638

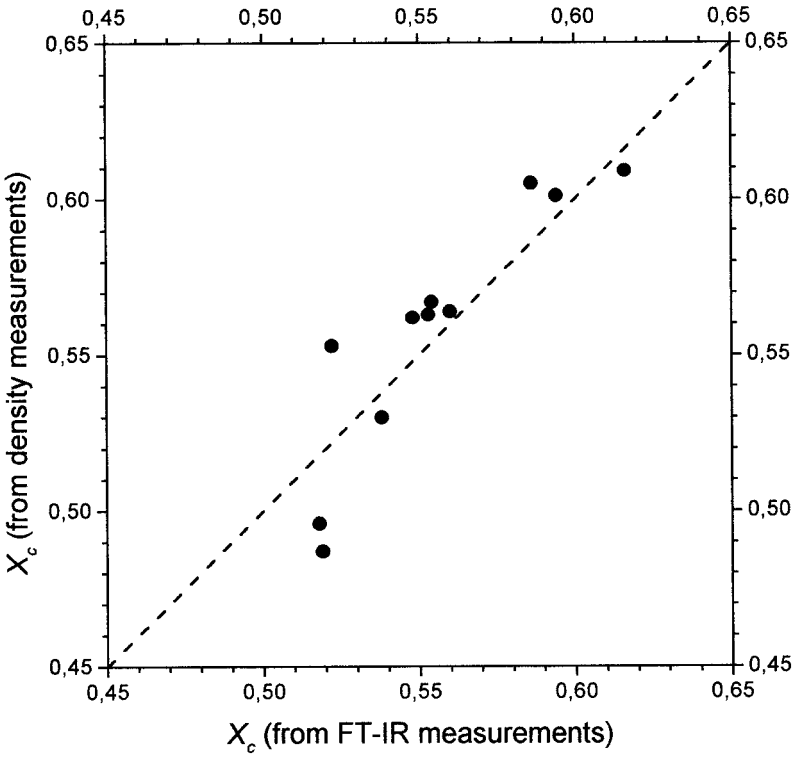

Figure 2 The density versus the FTIR measurements of the crystallinity of the iPP T30G sample that experienced different thermal histories.

ples as specified below. Crystallinities obtained by density measurements (setting ρ_c = 940 kg m^{-3} and ρ_{am} = 856 kg m^{-3}) were fitted by eq. (4); the best agreement was obtained by $a(\nu_c)/a(\nu_{am})$ = 0.57, which identifies the material absorptivity coefficient ratio. A comparison of the crystallinities obtained by density and FTIR measurements is shown in Figure 2 for $a(\nu_c)/a(\nu_{am})$ = 0.57.

The average (f_{av}) and crystalline phase (f_c) Hermans orientation factors were both determined by dichroism, adopting procedures described by Samuels.[20] To this purpose the absorbances of polarized IR radiation at ν_1 = 1220 cm^{-1} and ν_2 = 1256 cm^{-1} were measured for every sample. The dichroic ratio at a ν is defined as $D_\nu = (A_\pi/A_\sigma)_\nu$, where A_π is the absorbance when the polarization plane is parallel to the draw direction and A_σ is the absorbance when the polarization plane is orthogonal to the draw direction. (Both were obtained via suitable fitting of experimental spectra.) The relation between the Hermans factor of the crystalline phase and the dichroic ratio at ν_1 is

$$f_c = \left[\left(\frac{D-1}{D+2}\right)\left(\frac{D_0+2}{D_0-1}\right)\right]_{\nu_1} \quad (5)$$

While the absorption at ν_1 is characteristic of the crystalline phase,[20] ν_2 is related to a peak sensitive to the phase fraction average orientation, defined as[20]

$$f_{av} = f_c X_c + f_{am}(1 - X_c) \quad (6)$$

The average orientation factor is then:

$$f_{av} = \left[\left(\frac{D-1}{D+2}\right)\left(\frac{D_0+2}{D_0-1}\right)\right]_{\nu_2} \quad (7)$$

Dichroic ratios for total alignment are[20] D_{0,ν_1} = 2 cot^2 (72°) = 0.211 and D_{0,ν_2} = 2 cot^2 (38.5°) = 3.161. The f_c and f_{av} were determined on all films obtained under the conditions listed in Table II; once f_c and f_{av} and X_c are identified, f_{am} can be calculated by eq. (6).

MODEL OUTLINE

The film casting process is shown schematically in Figure 3; the stretching direction (usually

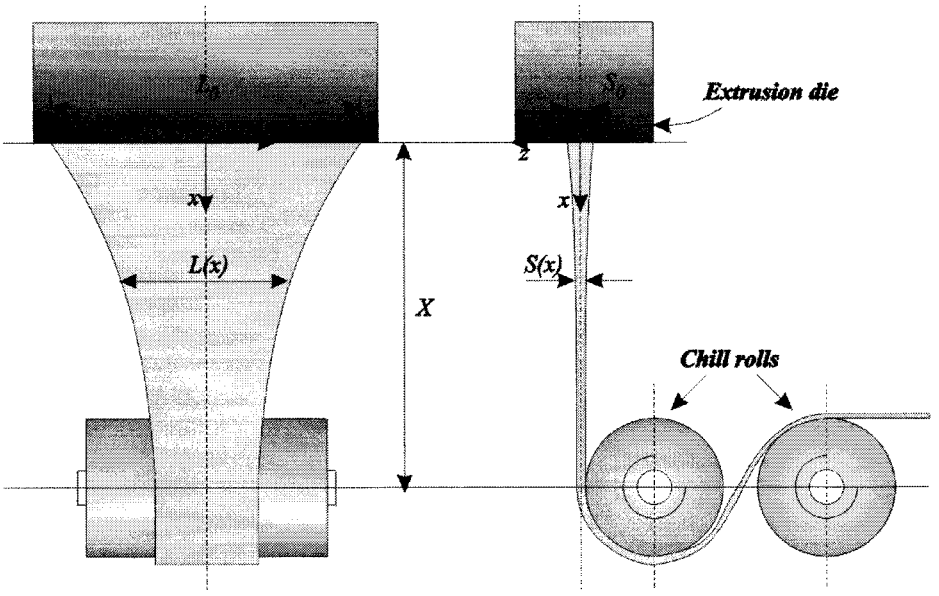

Figure 3 A scheme of the film casting experiment.

called the *machine direction* or *MD*), the width direction (usually called the *transverse direction* or *TD*), and the thickness direction are *x, y*, and *z*, respectively. The thermomechanical model of the film casting process was already reported[7]; the model was developed on the basis of the following simple kinematics:

$$\underline{\boldsymbol{v}}(x, y, z) = \begin{cases} v_x(x) \\ yf(x) \\ zg(x) \end{cases}$$

accounting for the mass, momentum, energy balances, corresponding boundary conditions, and free-surface conditions. The final equations are briefly summarized below:

$$\frac{dL}{dx} = \frac{6\mu\dot{m}}{\rho FL} - \sqrt{\left(\frac{6\mu\dot{m}}{\rho FL}\right)^2 + 2} \tag{8}$$

$$\frac{dv_x}{dx} = \frac{v_x}{4}\left(\frac{F\rho}{\mu\dot{m}} - \frac{2}{L}\frac{dL}{dx}\right) \tag{9}$$

$$\frac{dF}{dx} = \dot{m}\left(\frac{dv_x}{dx} - \frac{g}{v_x}\right) \tag{10}$$

$$\frac{dX_c}{dx} = \frac{[X_{\text{eq}} - X_c(x)]}{v_x} n \ln 2 \left[\int_0^x K(T(x))\frac{d\xi}{v_x}\right]^{n-1} K(T(x)) \tag{11}$$

$$\frac{dT}{dx} = \frac{2h_{\text{tot}}(T_a - T)L}{C_p\dot{m}} + \frac{\Delta H}{C}\frac{dX_c}{dx} \tag{12}$$

$$x = 0, \begin{cases} L = L_0 \\ v_x = v_{x0} \\ T = T_0 \\ X_c = 0 \end{cases} \quad x = X, \quad v_x = v_{xX} \tag{13}$$

where $L(x)$ is the film width, $v_x(x)$ is the velocity component along the draw direction (x), $F(x)$ is the force acting in the x direction, $T(x)$ is the film temperature, and $X_c(x)$ is the crystallinity. The material functions are the viscosity (μ), density (ρ), specific heat (C_p), latent heat of melting/crystallization (ΔH), and overall crystallization rate constant (K). The X_{eq} and n in eq. (11) are parameters of the crystallization kinetics model, and h_{tot} and T_a in eq. (12) are the total heat exchange coefficient and ambient (air) temperature. In eq. (13) the L_0, v_{x0}, and T_0 are values of the width, velocity, and temperature at the die, respectively, and v_{xX} is the take-up velocity. The symbols' meanings are reported in the notation Nomenclature section, and details on the solution procedure can be found elsewhere.[7]

The evolution of the end to end distance of macromolecules modeled as Hookean elastic dumbbells can be considered on the basis of kinematics obtained with the thermomechanical model summarized above. Denoting the chain end to end vector by $\underline{\mathbf{Q}}$, the evolution equation for the molecular conformation tensor $\underline{\mathbf{c}} = \langle\underline{\mathbf{QQ}}\rangle$ is[21]

$$\frac{\delta \underline{\underline{\mathbf{c}}}}{\delta t} = \frac{\underline{\underline{\mathbf{c}}}}{\partial t} + \nu \cdot \underline{\nabla \underline{\underline{\mathbf{c}}}} - \underline{\underline{\nabla \boldsymbol{\nu}^T}} \cdot \underline{\underline{\mathbf{c}}} - \underline{\underline{\mathbf{c}}} \cdot \underline{\nabla \nu} = \frac{4k_B T}{\zeta} \underline{\underline{\mathbf{I}}} - \frac{4H}{\zeta} \underline{\underline{\mathbf{c}}} \tag{14}$$

The solution of eq. (14) under quiescent and steady conditions is

$$\underline{\underline{\mathbf{c}_{\text{eq}}}} = \frac{k_B T}{H} \underline{\underline{\mathbf{I}}} = \frac{Q_{\text{eq}}^2}{3} \underline{\underline{\mathbf{I}}} \tag{15}$$

Adapting eq. (15) into eq. (14) leads to

$$\frac{\delta \underline{\underline{\mathbf{c}}}}{\delta t} = \frac{1}{\lambda} (\underline{\underline{\mathbf{c}_{\text{eq}}}} - \underline{\underline{\mathbf{c}}}) \tag{16}$$

where

$$\lambda = \frac{\zeta}{4H} \tag{17}$$

is the system relaxation time.

Adopting as variable the dimensionless conformation tensor

$$\underline{\underline{\mathbf{a}}} = \frac{3}{Q_{\text{eq}}^2} (\underline{\underline{\mathbf{c}}} - \underline{\underline{\mathbf{c}_{\text{eq}}}}) \tag{18}$$

the length of the dumbbell Q_{eq} under quiescent conditions disappears and eq. (16) simplifies to

$$\frac{\delta \underline{\underline{\mathbf{a}}}}{\delta t} = \underline{\underline{\nabla \boldsymbol{\nu}^T}} + \underline{\underline{\nabla \boldsymbol{\nu}}} - \frac{1}{\lambda} \underline{\underline{\mathbf{a}}} \tag{19}$$

The diagonal components of eq. (19) can be written as

$$\begin{cases} \dfrac{da_{xx}}{dx} = \dfrac{1}{\nu_x} \left[\left(2 \dfrac{d\nu_x}{dx} - \dfrac{1}{\lambda} \right) a_{xx} + 2 \dfrac{d\nu_x}{dx} \right], & a_{xx}\,(x = 0) = 0 \\ \dfrac{da_{yy}}{dx} = \dfrac{1}{\nu_x} \left[\left(2 \dfrac{\nu_x}{L} \dfrac{dL}{dx} - \dfrac{1}{\lambda} \right) a_{xx} + 2 \dfrac{\nu_x}{L} \dfrac{dL}{dx} \right], & a_{yy}\,(x = 0) = 0 \\ \dfrac{da_{zz}}{dx} = \dfrac{1}{\nu_x} \left[\left(2 \dfrac{\nu_x}{S} \dfrac{dS}{dx} - \dfrac{1}{\lambda} \right) a_{xx} + 2 \dfrac{\nu_x}{S} \dfrac{dS}{dx} \right], & a_{zz}\,(x = 0) = 0 \end{cases} \tag{20}$$

where, according to the model adopted, the velocity components are as follows (S is the film thickness):

$$\begin{cases} \nu_x = \nu_x(x) \\ \nu_y = yf(x) = y \dfrac{\nu_x(x)}{L} \dfrac{dL}{dx} \\ \nu_z = zg(x) = z \dfrac{\nu_x(x)}{S} \dfrac{dS}{dx} \end{cases} \tag{21}$$

The relation between the conformational tensor components and the Hermans factor can be drawn by starting from the definition of the Hermans factor:

$$f_H = \frac{3}{2} \langle \cos^2 \theta \rangle - \frac{1}{2} \tag{22}$$

where θ is the angle between the drawing direction and the axis of the dumbbell. Because the end to end vector in the reference frame is

$$\underline{\mathbf{Q}} = X\underline{\hat{\mathbf{i}}} + Y\underline{\hat{\boldsymbol{\jmath}}} + Z\underline{\hat{\mathbf{k}}} \tag{23}$$

the ith projection of vector $\mathbf{Q}$ can be written as

$$|\underline{\mathbf{Q}}| \cos\, \theta = X \tag{24}$$

$$\cos^2 \theta = \frac{X^2}{|\underline{\mathbf{Q}}|^2} \tag{25}$$

Averaging over the dumbbell population and adopting a "decoupling" approximation gives

$$\langle \cos^2 \theta \rangle = \left\langle \frac{X^2}{|\underline{\mathbf{Q}}|^2} \right\rangle \cong \frac{\langle X^2 \rangle}{\langle |\underline{\mathbf{Q}}|^2 \rangle} = \frac{c_{xx}}{\text{tr}(\underline{\underline{\mathbf{c}}})} \tag{26}$$

At last, using eq. (18) one can write

$$\langle \cos^2 \theta \rangle \cong \frac{a_{xx} + 1}{\text{tr}(\underline{\underline{\mathbf{a}}}) + 3} \tag{27}$$

and the Hermans factor becomes

$$f_H = \frac{3}{2}\langle\cos^2\theta\rangle - \frac{1}{2} = \frac{3}{2}\frac{a_{xx}+1}{tr(\underline{\underline{\mathbf{a}}})+3} - \frac{1}{2} \qquad (28)$$

Once $T(x)$, $v_x(x)$, and $L(x)$ are identified by the thermomechanical model [eqs. (8–12)], the components of the orientation tensor can be calculated by means of eq. (20) To this purpose, at each temperature the relaxation time $\lambda^*(T)$ was calculated in agreement with the "Spriggs' truncated power law," as reported by Bird et al,[22] in which the time constant is $\lambda^* = 1/\dot{\gamma}^*$, where $\dot{\gamma}^*$ is the value of the shear rate at which "shear thinning" begins.[22] In particular, if the quiescent relaxation time $\lambda^*(T)$ is identified as the reciprocal of the shear rate at which the viscosity attains a value μ^* equal to a fraction $1/\kappa$ of the Newtonian value, the Cross equation gives

$$\lambda^*(T) = (\kappa - 1)^{1/n_c - 1} C\mu_0(T) \qquad (29)$$

A κ value of 2.5 was adopted here for the determination of $\lambda^*(T)$.

The relaxation time of the flowing and crystallizing polymer was assumed to follow a viscosity dependence on the flow and crystallinity:

$$\lambda(T, \dot{\gamma}, X_c) = \lambda^*(T)\frac{\mu(T, \dot{\gamma}, X_c)}{\mu_0(T)} \qquad (30)$$

The relaxation time predicted by eq. (30), as the viscosity is predicted by eq. (1), accounts for the temperature, flow, and crystallinity dependencies; it is a parameter able to describe the behavior of a polymer melt flowing and crystallizing under isothermal and nonisothermal conditions. In this way eq. (19) can also predict the conformation evolution of the polymer during crystallization.

RESULTS

A thermomechanical model was previously shown to correctly predict the width and temperature distribution in the film casting process.[7,8] Nevertheless, a comparison of the width and temperature data with model predictions is shown in Figure 4 with reference to runs H1 and H2 whose operating conditions are reported in Table II.

As shown in Figure 4, the model predictions are in agreement with the experimental data. Small differences between the model predictions and experiments may be related to either inaccuracy of the rheological characterization or to underestimation of the heat flux in the lower part of the film. Furthermore, the crystallization kinetics adopted does not account for the effect of the flow on the crystallization. Nevertheless, model predictions lead to sufficiently accurate values of temperature and velocity distributions, which are the starting point for computation of conformational tensor evolution.

The orientation factors of the final films are reported in Figures 5 and 6 versus the DR. The data of Figures 5 and 6 show a sudden increase of the crystalline orientation factor at a critical draw ratio. The values of this critical draw ratio are however different in the two figures, which group data taken with two different die thicknesses. The experimental amorphous orientation data undergo only a slight increase with the draw ratio; consequently, at high *DR* the amorphous phase is thus much less oriented than the crystalline phase. Obviously, average orientation is intermediate between f_c and f_{am}.

It must be stressed that the critical draw ratio does not appear appropriate to identify the onset of residual orientation. Its value is indeed different in the two figures: it lies between 10 and 15 in Figure 5, while it lies between 20 and 22 in Figure 6.

The orientation factors predicted by the dumbbell model at the *frozen line* (i.e., the distance from the die where crystallinity reaches a few percent and the film width no longer changes) are also reported in Figures 5 and 6. Predictions of the melt orientation factor at the frozen line obtained using the dumbbell model gradually increase with the draw ratio from zero to one and a critical *DR* is not identified. The only way for the model of the orientation evolution to agree with the data in Figures 5 and 6 is that there is an *experimentally evidenced* onset of the melt orientation factor of about 0.6 for developing crystallization toward highly oriented structures.

By contrast, for values of the melt orientation factor smaller than about 0.6, the polymer would crystallize toward unoriented structures. Such an onset as evidenced in Figures 5 and 6 should be described in a flow induced crystallization model.

The thermomechanical model also provides stress distribution in the film and in particular at the frozen line position. The orientation factors of the crystalline phase are reported in Figure 7 versus the calculated stress level at the frozen line [σ_{xx} ($x = x_{FL}$)] for both series of runs (G and

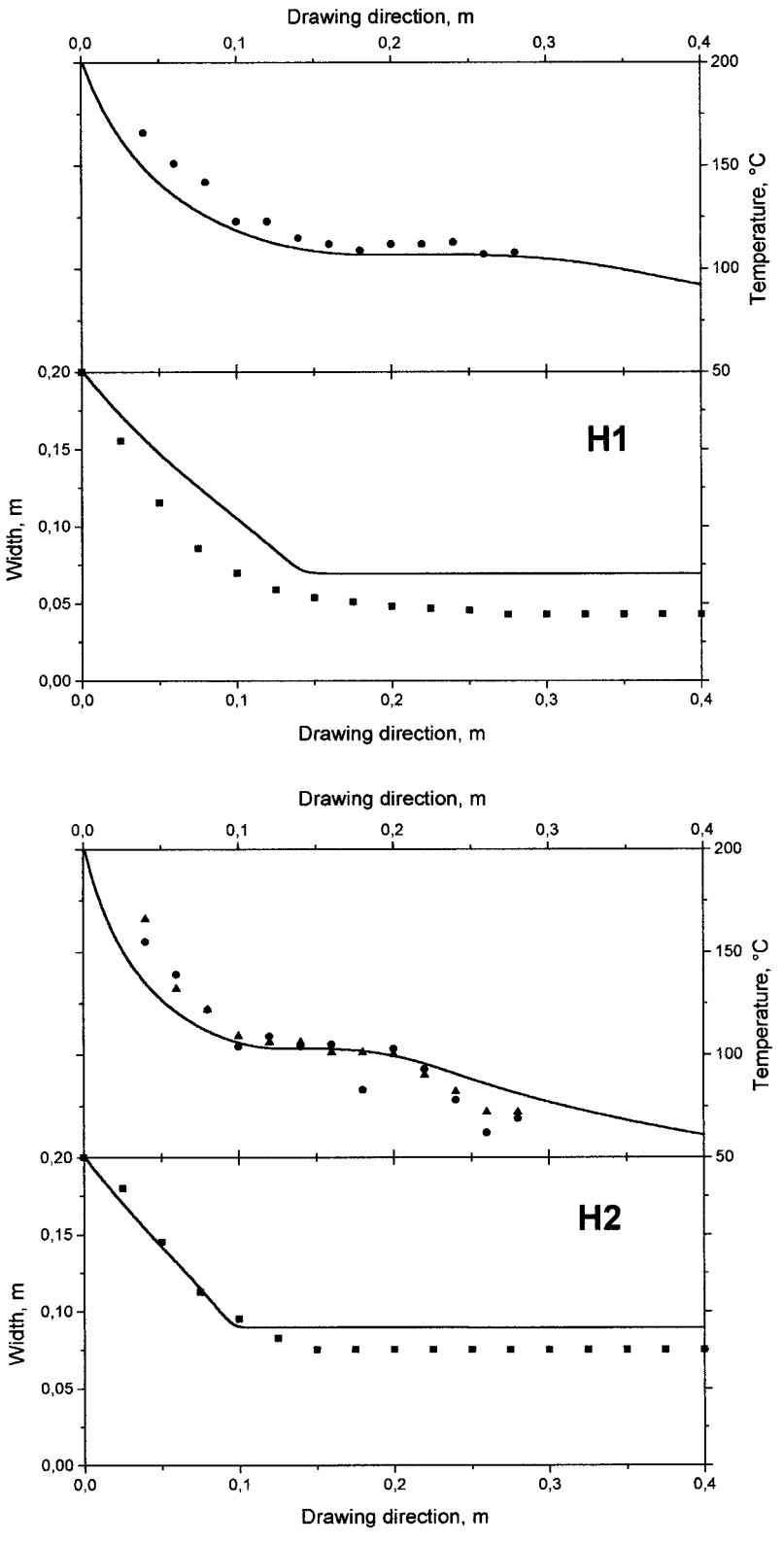

Figure 4 The width and temperature distribution along the drawing direction for runs H1 and H2 characterized in Table II. (—) The model predictions and (●, ■, ▲) the experimental values.

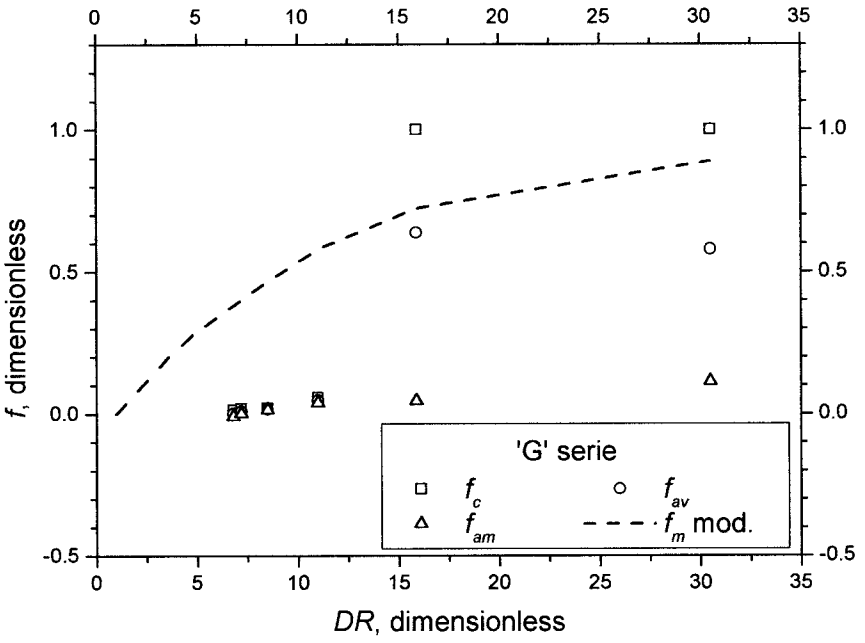

Figure 5 The Hermans orientation factors; the experimental values of final films f_c, f_{am}, and f_{av}; and the prediction of the model at the frozen line (f_m) versus the draw ratio for runs of series G.

H). Both series of data show a steep increase of the crystalline orientation for a value of the stress calculated at the frozen line of about 250 kPa, which appears to be a critical stress level for the development of oriented crystallization. Also, predictions of the melt orientation factor at the frozen line collapse into a single curve if plotted versus the stress level at the frozen line rather than versus the *DR*.

It is well known that molecular orientation enhances the crystallization kinetics of polymers; as a consequence, solidification of an oriented melt would lead to a final crystallinity larger than that achieved without orientation under the same cooling history. Cooling histories during the film casting process were calculated by the model, and final crystallinities were measured by the FTIR method as described in the Experimental section. These data can be compared with those obtained from samples cooled under quiescent conditions at the same cooling rate.[17] Although the cooling rate is not constant during quiescent quenching experiments, as well as along the cast film process, a suitable cooling rate, characterizing the region of the cooling history relevant for crystallization, is well approximated by the value assumed in an appropriate narrow range of temperatures, which for iPP was found[23] to be in the neighborhood of 70°C. The cystallinities measured on the same material under quiescent conditions and those of series H are reported in Figure 8 versus the cooling rate at 70°C.

The effect of flow on the crystallization kinetics is clearly shown: the observed final crystallinity of films of series H is certainly larger than the crystallinity of samples solidified in quiescent conditions at the same cooling rate. Moreover, the crystallinity index value of cast films is close to the value that the crystallinity index attains under quiescent conditions but at cooling rates more than 1 order of magnitude lower.

CONCLUSIONS

The Hermans orientation factors of the crystalline phase measured on films obtained under different conditions (DR, initial thickness, take-up distance) show on increase from very low to very high values as the DR increases. Further, if the crystalline phase orientation factor is plotted versus the stress at the frozen line, it undergoes a sudden change from very low values to values close to one at a critical stress level, suggesting the existence of a threshold value of this variable in order for flow effects on crystallization kinetics to take place.

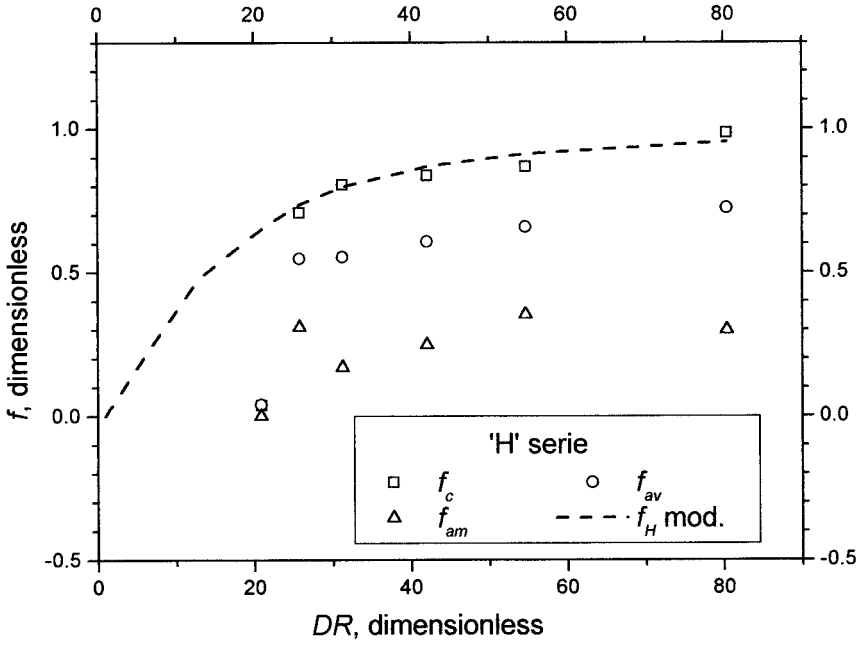

Figure 6 The Hermans orientation factors; the experimental values of final films f_c, f_{am}, and f_{av}; and the prediction of the model at the frozen line versus the draw ratio for runs of series H.

The melt orientation factor, calculated by the Hookean dumbbell model, also shows the same behavior (i.e., collapse into a single curve), irrespective of changes applied to operating conditions, if plotted versus the stress at the frozen line. This result coupled with the crystalline

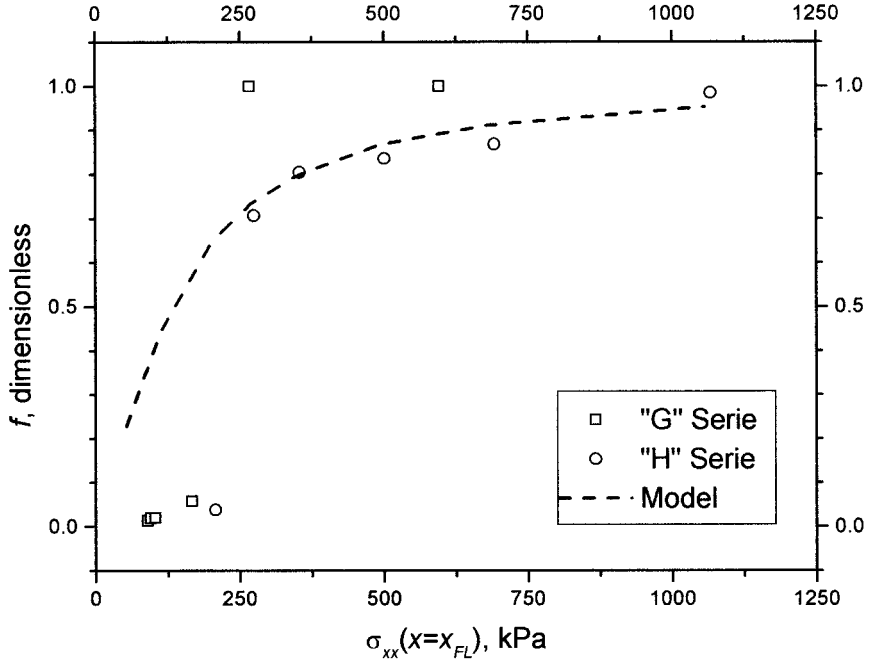

Figure 7 The experimental orientation factor of the crystalline phase in final films and model predictions for the orientation factor at the frozen line versus the stress at the frozen line.

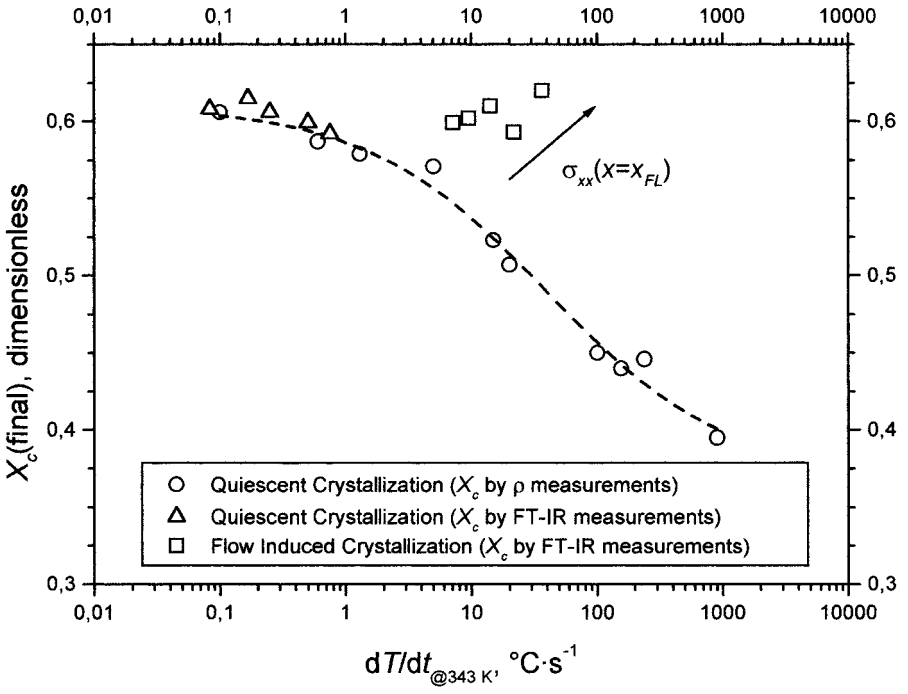

Figure 8 The crystallinity in the final samples versus a characteristic cooling rate.

phase orientation behavior strongly suggests the adoption of stress as a relevant variable in the modeling of the effects of flow on the crystallization kinetics, at least under elongational flow.

Hermans orientation factor of the amorphous phase measured on films obtained in different conditions (*DR*, initial thickness, take-up distance) showed negligible or quite low values (series H) according to general literature data.[24]

The crystallinity index values of the final films were found to be larger than the crystallinity index values obtained under quiescent conditions at the same cooling rate, showing that flow induced crystallization effects are relevant in the conditions adopted for the experiments.

NOMENCLATURE

a	FTIR absorptivity coefficient (arbitrary units)
A	FTIR absorbance (arbitrary units)
C_p	specific heat of polymer (kJ kg^{-1} K^{-1})
D, D_0	dichroic ratios (dimensionless)
DR	draw ratio = ν_{xX}/ν_{x0} (dimensionless)
f, f_H	Hermans orientation factors (dimensionless)
F	draw force (x component of force acting on the polymer) (N)
H	friction parameter in dumbbell model (N m^{-1})
K	rate of crystallization function (s^{-1})
$L(x)$, L	film width distribution along draw direction, actual film width (m)
L_0	initial value of film width (width of die) (m)
$\dot{m}$	mass flow rate of polymer (kg s^{-1})
n	Avrami exponent (dimensionless)
$S(x)$, S	film thickness distribution along draw direction, actual film thickness (m)
S_0	initial value of film thickness (thickness of die) (m)
t	time (s)
T	temperature of polymer (K or °C)
T_0	extrusion temperature (K or °C)
T_a	surrounding temperature (ambient) (K or °C)
ν_x	x component of velocity (ms^{-1})
ν_{x0}	initial value (at $x = 0$) for the x component of velocity (ms^{-1})
ν_{xX}	final value (at $x = X$) for x component of velocity (ms^{-1})
x	coordinate in stretching direction (m)
x_{FL}	frozen-line position (m)

X take-up distance (m)
X_c volumetric degree of crystallinity (dimensionless)
X_{eq} final or equilibrium volumetric degree of crystallinity (dimensionless)

Greeks

ΔH latent heat of crystallization for iPP (kJ kg^{-1})
λ relaxation time (s)
μ material viscosity (Pas)
ν wavenumber (cm^{-1})
ρ materials' density (kgm^{-3})
θ angle between axis of dumbbell and drawing direction (rad)
σ components of stress tensor (Pa)
ζ friction parameter in dumbbell model (Nsm^{-1})

Subscripts and Superscripts

am amorphous phase
av phase average
c crystalline phase
eq quiescent and steady conditions

Vectors and Tensors

$\underline{\mathbf{Q}}$ chain end to end vector in dumbbell model (m)
$\underline{\boldsymbol{\nu}}$ velocity (ms^{-1})
$\underline{\underline{\mathbf{a}}}$ dimensionless molecular conformational tensor (dimensionless)
$\underline{\underline{\mathbf{c}}}$ molecular conformational tensor (m^2)

REFERENCES

1. Pearson, J. R. A. Mechanical Principles of Polymer Melt Processing; Pergamon: Oxford, UK, 1966.
2. Narayanaswamy, O. S. J Am Ceram Soc 1977, 60, 1.
3. Agassant, J. F.; Avenas, P.; Sergent, J. Ph.; Carreau, P. J. Polymer Processing. Principles and Modelling; Hanser: New York, 1977.
4. Duffo, P.; Monasse, B.; Haudin, J. M. J Polym Eng 1991, 10, 151.
5. Barq, P.; Haudin, J. M.; Agassant, J. F. Int Polym Process 1992, VII, 334.
6. Acierno, D.; Di Maio, L.; Ammirati, C. C. Polym Eng Sci 2000, 40, 108.
7. Lamberti, G.; Titomanlio, G.; Brucato, V. Chem Eng Sci 2001, 56, 5749.
8. Lamberti, G.; Titomanlio, G.; Brucato, V. Chem, Eng Sci, to appear.
9. Lagasse, R. R.; Maxwell, B. Polym Eng Sci 1976, 16, 189.
10. McHugh, A. J. Polym Eng Sci 1982, 22, 15.
11. Coppola, S.; Grizzuti, N.; Maffettone, P. L. Macromolecules 2001, 34, 5030.
12. Eder, G.; Janeschitz-Kriegl, H. In Materials Science and Technology; Meijer, H. E. H., Ed.; Wiley: New York, 1997; Vol. 18.
13. Doufas, A. K.; McHugh, A. J.; Miller, C. J Non-Newtonian Fluid Mech 2000, 92, 27.
14. Doufas, A. K.; McHugh, A. J.; Miller, C.; Immaneni, A. J Non-Newtonian Fluid Mech 2000, 92, 27.
15. Nobile, M. R., personal communication, 2001.
16. Titomanlio, G.; Speranza, V.; Brucato, V. Int Polym Proc 1997, 12.
17. Piccarolo, S.; Brucato, V.; Foresta, T.; LaCarrubba, V. In Proceedings of PPS15 on CD-ROM; Anderson, P. D., and Kruijt, P. G. M., Eds.; Hertogenbosh: The Netherlands, 1999.
18. Nakamura, K.; Watanabe, T.; Katayama, K.; Amano, T. J Appl Polym Sci 1972, 16, 107.
19. Ward, I. M. Structure and Properties of Oriented Polymers; Chapman & Hall; London, 1997.
20. Samuels, R. J. Structured Polymer Properties; Wiley: New York, 1974.
21. Bird, R. B.; Curtiss, C. F.; Armstrong, R. C.; Hassager, O. Dynamics of Polymeric Liquids, Vol. 2: Kinetic Theory; Wiley: New York, 1987.
22. Bird, R. B.; Armstrong, R. C.; Hassager, O. Dynamics of Polymeric Liquids, Vol. 1: Fluid Mechanics; Wiley: New York, 1987.
23. Piccarolo, S.; Alessi, S.; Brucato, V.; Titomanlio, G. In Crystallization of Polymers; M., Ed; Dosiere, M., Ed; NATO ASI Series; Kluwer: New York, 1983.
24. Ziabicki, A.; Kawai, H. High Speed Fiber Spinning; Wiley: New York, 1985.